JOURNAL OF SOLID STATE CHEMISTRY 71, 131–138 (1987)

Crystal Structure and Magnetic Properties of a New Molybdenophosphate: $AgMo_5P_8O_{33}$

K.-H. LII, D. C. JOHNSTON, D. P. GOSHORN, AND R. C. HAUSHALTER

Corporate Research Science Laboratories, Exxon Research and Engineering Company, Route 22 East, Annandale, New Jersey 08801

Received November 14, 1986; in revised form January 15, 1987

The crystal structure of $AgMo_5P_8O_{33}$ has been determined from single-crystal X-ray diffraction data. $AgMo_5P_8O_{33}$ crystallizes in the monoclinic space group $I2/a$ (#15) with $a = 23.050(8)$, $b = 4.831(4)$, $c = 22.935(9)$ Å, $\beta = 90.42(5)°$, $V = 2554(4)$ Å^3, $Z = 4$, $R = 0.086$ ($R_w = 0.089$) for 879 reflections with $F_o^2 > 3.0\sigma(F_o^2)$. The structure consists of large tunnels where the silver atoms are located. The framework is built up from MoO_6 octahedra and P_2O_7 groups. The connectivity formula for $AgMo_5P_8O_{33}$ is $Ag(MoO_{1/1}O_{4/2})(MoO_{1/1}O_{5/2})_4(P_2O_{1/1}O_{6/2})_4$. Powder magnetic susceptibility data confirm the presence of Mo^{5+} (d^1) ions with spin ½, and a featureless antiferromagnetic ordering appears to occur below 2.5 K. Magnetization isotherms at 1.3 and 4.2 K in magnetic fields up to 65 kG are reported. The lithium, sodium, calcium, strontium, barium, and lead analogs of $AgMo_5P_8O_{33}$ were also prepared.

Introduction

In the quaternary system M–Mo–P–O (M = metal cation), a variety of frameworks which are composed from corner-sharing MoO_6 octahedra and PO_4 tetrahedra have been observed. The prominent features of these frameworks are tunnels or gaps in which the counter cations are located. For example, the compounds $Cs_4Mo_8P_{12}O_{52}$ and $Cs_2Mo_4P_6O_{26}$ are composed of the same building units, but these units are arranged in different ways so that tunnel and layer structures, respectively, result (*1*). The potassium, rubidium, and thallium analogs of $Cs_4Mo_8P_{12}O_{52}$ also exist. Two different, but closely related, polymorphs of $K_4Mo_8P_{12}O_{52}$ have also been observed (*1, 2*). Our previous work showed that the "$Mo_8P_{12}O_{52}$" framework in the $Cs_4Mo_8P_{12}O_{52}$ structure was flexible and that the size of the tunnel was dependent upon the size of the counter cation (*1*). In an attempt to prepare isostructural compounds containing counter ions smaller than K^+, a new structure type has been discovered. In this paper we present the preparation, crystal structure, and magnetic properties of $AgMo_5P_8O_{33}$. The lithium, sodium, calcium, strontium, barium, and lead analogs of $AgMo_5P_8O_{33}$ were also prepared.

Experimental and Results

Preparation and Characterization

All manipulations were performed under an He atmosphere. MoO_2 (99.9%), MoO_3

0022-4596/87 $3.00

(99.9%), Na_2MoO_4 (99.9%), Li_2MoO_4 (99.9%), $BaMoO_4$ (99.9%), and $PbMoO_4$ (99.9%) were purchased from Cerac. CaO (99.95%), SrO (99.5%), and Ag_2O (99.7%) were from AESAR, Alfa, and Matheson, Coleman and Bell, respectively. X-ray powder diffraction patterns for identification purposes were obtained using a Philips powder diffractometer and filtered copper radiation. Each sample was contained in a vacuum-tight cell which was fitted with a Be window.

A reaction aiming at "$Ag_4Mo_8P_{12}O_{52}$" at 950°C yielded some small green needle crystals which were apparently a new phase based on the X-ray powder pattern. The exact stoichiometry of the green crystal was not known until its single-crystal X-ray structure was solved. Subsequently, a pure product $AgMo_5P_8O_{33}$ was obtained by heating a mixture of proper stoichiometry of Ag_2O, MoO_3, MoO_2, and P_2O_5 in a sealed quartz tube at 860°C for 2 days.

On the basis of X-ray analysis, pure $MMo_5P_8O_{33}$ (M = Li, Na) compounds were obtained by heating stoichiometric mixtures of the starting materials at 800°C in sealed quartz tubes for several days. The unit cell parameters for single crystals of $LiMo_5P_8O_{33}$ and $NaMo_5P_8O_{33}$, determined by using a Rigaku AFC6-R rotating anode diffractometer, were I-centered monoclinic, a = 22.765(7), b = 4.853(2), c = 22.951(8) Å, β = 91.17(3)°, V = 2534.8(15) Å^3 and I-centered monoclinic, a = 22.95(1), b = 4.853(1), c = 23.08(1) Å, β = 90.39(3)°, V = 2571(3) Å^3, respectively. Attempts to prepare pure $MMo_5P_8O_{33}$ (M = Ca, Sr, Ba, Pb) (890°C, 3–7 days) were also performed, but each of the X-ray powder patterns showed a few unindexed reflections and a small amount of MoO_2. A green needle crystal of the barium compound was indexed on the same four-circle diffractometer and gave the following cell parameters: I-centered monoclinic, a = 23.034(8), b = 4.830(2), c = 23.218(10) Å, β = 90.90(3)°, V = 2582.8(20) Å^3.

Single-Crystal X-Ray Structure Determination for $AgMo_5P_8O_{33}$

Data Collection

A fragment of a green needle crystal of $AgMo_5P_8O_{33}$ having approximate dimensions of 0.05 × 0.05 × 0.10 mm was mounted in a capillary tube in a random orientation. All measurements were made on a Rigaku AFC6R rotating anode diffractometer with monochromatic MoK_α radiation. Omega scans of several intense reflections had an average width at half-height of 0.2° with a takeoff angle of 6.0°, indicating good crystal quality. The cell constants were obtained at 23°C from 15 carefully centered reflections in the range $10.0° < 2\theta < 15.0°$. An I-centered monoclinic cell with dimensions a = 23.050(8), b = 4.831(4), c = 22.935(9) Å, β = 90.42(5)° was chosen so that the interaxial angle β was as near 90° as possible. In order to verify that this was the correct unit cell, each axis was artificially doubled and a subset of low-angle data was collected, but there was no evidence for a doubling of any axis. Based on the systematic extinctions of hkl: $h + k + l = 2n + 1$; $h0l$: $h, l = 2n + 1$, and the successful solution and refinement of the structure, the space group was determined to be $I2/a$. The unit cell is nearly metrically tetragonal. The following evidence supports the choice of a monoclinic space group over the tetragonal space group ($I4_1/a$): (1) The β-angle has a significant deviation of 0.4° from 90°. This was observed for all crystals surveyed and was observed on the Rigaku AFC6R diffractometer with both Mo and Cu radiation and on the Enraf–Nonius CAD4 with Mo radiation. (2) The (020) reflection was observed at the 20σ (on F) level. In the tetragonal space group $I4_1/a$ this would be the (002) reflection and would be systematically ab-

sent. The reflection was measured at several different psi values to prove that it was not a multiple reflection. (3) The model that was developed in *I2/a* could not be transformed to fit the symmetry of $I4_1/a$.

Data Reduction

Of the 6096 reflections which were collected, 3304 were unique. The intensities of three standard reflections, which were measured after every 150 measured reflections, remained constant throughout the data collection. An empirical absorption curve calculated from three psi-scan reflections was essentially flat, therefore no absorption correction was applied. The data were corrected for Lorentz and polarization effects. The secondary extinction parameter (4.0×10^{-8}) was not included in the refinement.

Structure Solution and Refinement

The structure was solved by direct methods and Fourier techniques. Neutral atomic scattering factors were taken from Cromer and Waber (*3*). Anomalous dispersion effects were included in F_c (*4*); the values for $\Delta f'$ and $\Delta f''$ were those of Cromer (*5*). Only the Ag atoms were refined anisotropically, but they showed large thermal parameters in the *b* direction. There are two major Ag sites in the asymmetric unit. Other minor sites may be present but a better model could not be developed. The occupancy factors of the two major Ag sites were initially refined but the resultant values were very close to 0.25. In the final cycles of refinement, the occupancy factors were both fixed at 0.25. The last cycle of full-matrix least-squares refinement converged at $R = 0.086$ and $R_w = 0.089$. The relatively high *R*-factors and the inability to refine the nonsilver atoms anisotropically are probably related to the incomplete modeling of the disordered Ag atoms. It should also be noted that even with a rotating anode X-ray source only 27% of the reflections were observed ($I > 3\sigma(I)$).

The experimental details are listed in Table I. Positional parameters and B_{eq} are tabulated in Table II. Selected bond distances are given in Table III. Tables of observed and calculated structure factor amplitudes and listings of bond angles are available on request from the authors.

Magnetic Measurements

Magnetic susceptibility data were obtained from 4 to 300 K at a temperature sweep rate of less than 1 K/min in a magnetic field (*H*) of 6.3 kG using a George Associates Faraday Magnetometer under computer control. Additional magnetization data were obtained from 1.3 to 100 K in fields up to 65 kG using a PAR vibrating sample magnetometer.

The contributions of ferromagnetic impurities to the measured Faraday magne-

TABLE I

SUMMARY OF CRYSTAL DATA, INTENSITY MEASUREMENTS, AND STRUCTURE REFINEMENT PARAMETERS FOR $AgMo_5P_8O_{33}$

1. Crystal data	
Space group	*I2/a*
Cell parameters (296 K)	$a = 23.050(8)$ Å
	$b = 4.831(4)$ Å
	$c = 22.935(9)$ Å
	$\beta = 90.42(5)°$
	$V = 2554(4)$ Å^3
Z	4
Density (calc)	3.55 g/cm^3
Crystal size	0.05 × 0.05 × 0.10 mm
Absorption coefficient	37.07 cm^{-1}
2. Intensity measurements	
Radiation	MoK_α ($\lambda = 0.71069$ Å)
Scan mode	$\theta/2\theta$
Scan rate (in omega)	16°/min
Scan width (degree)	0.66 + 0.30 tan θ
Maximum 2θ	55.2°
No. of reflections measured	6096 total, 3304 unique
3. Structure solution and refinement	
Reflections included	879 with $F_0^2 > 3.0\sigma(F_0^2)$
Parameters refined	111
Agreement factors[a]	$R = 0.086$, $R_w = 0.089$
Esd of obs. of unit weight[b]	1.59
Max. peak in final difference map	2.90 e/Å^3 (at a distance of 0.7 Å from Mo2)

[a] $R = \Sigma||F_o| - |F_c||/\Sigma|F_o|$; $R = \text{SQRT}(\Sigma w(|F_o| - |F_c|)^2/\Sigma wF_o^2)$ with $w = 4F_o^2/\sigma^2(F_o^2)$.

[b] Esd of obs. of unit weight = $\text{SQRT}[\Sigma w(|F_o| - |F_c|)^2/(N_o - N_v)]$, where N_o = number of observations and N_v = number of variables.

TABLE II

POSITIONAL PARAMETERS AND B_{eq} FOR $AgMo_5P_8O_{33}$

Atom	x	y	z	B_{eq}[a]
Ag1	0.506(1)	0.44(1)	0.247(1)	4(2)
Ag2	0.505(2)	0.66(2)	0.258(1)	6(2)
Mo1	0.3425(1)	0.102(1)	0.3043(1)	0.13(7)
Mo2	0.4458(1)	0.3564(9)	0.0930(1)	0.14(7)
Mo3	1/4	0.989(1)	0	0.5(1)
P1	0.3755(4)	0.608(3)	0.2118(4)	0.4(2)
P2	0.3490(4)	0.846(3)	0.1013(4)	0.2(2)
P3	0.3521(4)	−0.395(3)	0.4011(4)	0.3(2)
P4	0.5389(4)	0.859(3)	0.1262(4)	0.5(2)
O1	0.362(1)	−0.110(7)	0.376(1)	0.5(5)
O2	0.321(1)	0.411(7)	0.359(1)	0.9(6)
O3	0.277(1)	−0.008(7)	0.293(1)	1.4(6)
O4	0.430(1)	0.275(7)	0.320(1)	0.7(6)
O5	0.388(1)	−0.166(7)	0.255(1)	1.1(6)
O6	0.341(1)	0.373(8)	0.238(1)	1.5(6)
O7	0.429(1)	0.533(6)	0.182(1)	0.4(5)
O8	0.335(1)	0.729(7)	0.164(1)	1.4(6)
O9	0.387(1)	0.661(7)	0.070(1)	0.4(5)
O10	0.290(1)	0.875(7)	0.071(1)	1.0(5)
O11	0.324(1)	−0.389(7)	0.462(1)	0.4(5)
O12	0.415(1)	−0.518(7)	0.417(1)	1.2(6)
O13	0.458(1)	0.229(6)	0.028(1)	0.2(5)
O14	0.508(1)	0.639(8)	0.091(1)	1.5(6)
O15	0.374(1)	0.117(7)	0.113(1)	0.9(5)
O16	0.496(1)	0.085(6)	0.141(1)	0.3(5)
O17	1/4	1.38(1)	0	1.6(8)

[a] The isotropic equivalent thermal parameter is defined as $B_{eq} = (\frac{4}{3})[a^2\beta_{11} + b^2\beta_{22} + c^2\beta_{33} + 2ab(\cos\gamma)\beta_{12} + 2ac(\cos\beta)\beta_{13} + 2bc(\cos\alpha)\beta_{23}]$.

tizations M were determined at several temperatures above 77 K from $M(H)$ isotherms with $H \leq 7.8$ kG and were found to be small, corresponding to about 40 atomic ppm of ferromagnetic iron metal impurities with respect to Mo; this contribution has been corrected for in the Faraday susceptibility data to be presented. The sample was loaded into a precalibrated vacuum-tight sample holder which was sealed in a He-filled dry box.

The magnetic susceptibility, χ, obtained using the Faraday magnetometer is plotted versus temperature from 4.2 to 290 K in Fig. 1a. These data were least-squares fitted from 4 to 290 K to the relation

$$\chi = \chi_0 + C/(T - \theta), \quad (1)$$

consisting of a temperature-independent contribution χ_0 and a Curie–Weiss contribution from the Mo^{5+} (d^1) magnetic moments. The solid curve in Fig. 1a is the fit, where $\chi_0 = -3.50 \times 10^{-7}$ cm^3/g, the Curie constant $C = 1.272 \times 10^{-3}$ cm^3 K/g, and the Weiss temperature $\theta = -0.4$ K. From the relation

$$C = \frac{N\mu_{eff}^2}{3k_B}$$

one obtains the effective moment $\mu_{eff} = 1.67\ \mu_B$/Mo. Using the relation $\mu_{eff} = g\sqrt{S(S+1)}\ \mu_B$ and spin $S = \frac{1}{2}$, the Landé factor is found to be $g = 1.93$. This value is slightly less than the free electron value 2.00, as is often found for Mo^{5+} coordinated by oxygen. The inverse susceptibility data, corrected for the χ_0 value above, are plotted in Fig. 1b, where the solid line is the above fit.

TABLE III

SELECTED INTERATOMIC DISTANCES (Å) IN $AgMo_5P_8O_{33}$

Atom	Atom	Distance	Atom	Atom	Distance
Ag1	O7	2.35(3)	Mo3	O17	1.90(6)
Ag1	O5	2.50(4)	Mo3	O10	1.95(3)
Ag1	O4	2.55(4)	Mo3	O10	1.95(3)
Ag1	O16	2.66(5)	Mo3	O11	1.98(2)
Ag1	O4	2.69(5)	Mo3	O11	1.98(2)
Ag2	O16	2.34(4)	P1	O7	1.47(3)
Ag2	O4	2.41(4)	P1	O5	1.50(3)
Ag2	O7	2.53(4)	P1	O6	1.51(4)
Ag2	O7	2.73(6)	P1	O8	1.54(3)
Ag2	O5	2.82(7)	P2	O9	1.45(3)
Mo1	O3	1.62(3)	P2	O15	1.45(3)
Mo1	O1	2.00(3)	P2	O10	1.53(3)
Mo1	O6	2.00(3)	P2	O8	1.59(3)
Mo1	O2	2.01(3)	P3	O1	1.51(3)
Mo1	O4	2.22(3)	P3	O11	1.54(3)
Mo2	O13	1.64(2)	P3	O12	1.60(3)
Mo2	O14	1.99(3)	P4	O4	1.47(3)
Mo2	O9	2.06(3)	P4	O14	1.50(3)
Mo2	O16	2.07(3)	P4	O16	1.51(3)
Mo2	O15	2.07(3)	P4	O12	1.57(3)
Mo2	O7	2.24(3)			

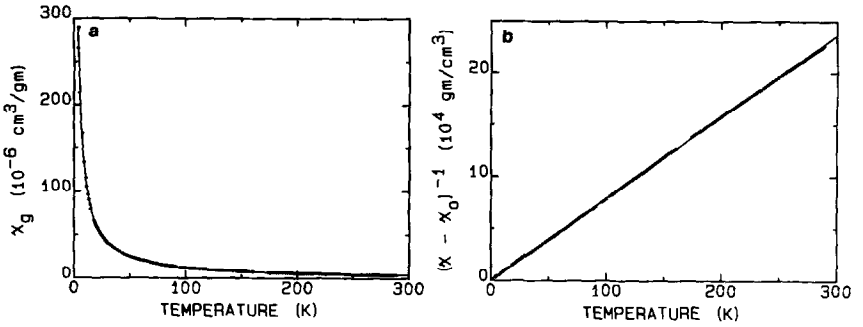

FIG. 1. (a) Gram magnetic susceptibility (χ_g) of $AgMo_5P_8O_{33}$ vs temperature. (b) Inverse gram magnetic susceptibility $(\chi - \chi_0)^{-1}$ of $AgMo_5P_8O_{33}$ vs temperature. The solid lines represent a least-squares fit to the data from 4.2 to 250 K according to Eq. (1).

The inverse susceptibility data obtained below 4.2 K in a field of 2 kG using the vibrating sample magnetometer are plotted in Fig. 2. From the fit to Eq. (1) from 2.5 to 4.2 K (solid line in Fig. 2), one obtains a more accurate Weiss temperature than in Fig. 1: $\theta = -1.0$ K. The magnetization data obtained at 1.3 and 4.2 K up to 65 kG are plotted versus reduced field $\mu_B H/k_B(T - \theta)$ in Fig. 3, where $\theta = -1.0$ K from Fig. 2. As seen in Fig. 3, the data at the two temperatures do not fall on a common curve; this indicates that below 4 K, the effective θ is both field- and temperature-dependent. It is thus not surprising that neither data set is well-described by a Brillouin function B_S for spin $S = \frac{1}{2}$ and $g = 1.93$, with the usual $B_S(H/T)$ replaced by $B_S(H/(T - \theta))$ to take into account the existence of a nonzero θ (solid curve in Fig. 3). The expected (high-field) saturation moment is $M_{sat} = gS\mu_B/\text{Mo} = 0.97\ \mu_B/\text{Mo}$; the data at high field in Fig. 3 appear to be approaching this limit. From the sign and magnitude of θ, one might expect antiferromagnetic order to set in below a Néel temperature $T_N \lesssim 1$ K. Indeed, a deviation of the data of the expected sign does occur from the Curie–Weiss fit in Fig. 2 below 2.5 K. However, no sharp features are seen in Fig. 2 above 1.3 K, suggesting that short-range (spin glass-like) ordering may be setting in below 2.5 K.

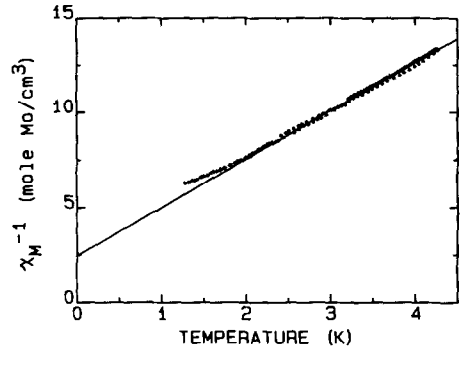

FIG. 2. Inverse molar magnetic susceptibility (χ_M^{-1}) for $AgMo_5P_8O_{33}$ in the temperature range 1.3 to 4.2 K. The solid line is a fit of Eq. (1) to the data from 2.5 to 4.2 K, with $\chi_0 \equiv 0$.

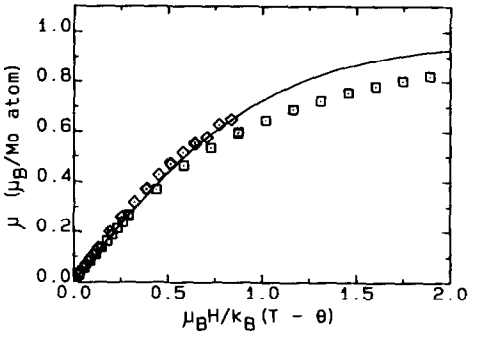

FIG. 3. Magnetization per molybdenum ion (μ) vs reduced magnetic field $\mu_B H/k_B(T - \theta)$ for $AgMo_5P_8O_{33}$ at 1.3 (squares) and 4.2 K (diamonds) in fields (H) up to 65 kG. The solid line is the Brillouin function $B_S(H/(T - \theta))$ for spin $S = \frac{1}{2}$, Landé factor $g = 1.93$, and $\theta = -1.0$ K.

Description and Discussion of the Structure

Figure 4 shows a view of the $AgMo_5P_8O_{33}$ structure down the monoclinic *b* axis. Each unit cell contains four large tunnels where the silver atoms are located. The tunnels are interlinked by the O–Mo3–O bonds (see Fig. 5). In contrast to $Cs_4Mo_8P_{12}O_{52}$, $Cs_2Mo_4P_6O_{26}$, α- and β-$K_4Mo_8P_{12}O_{52}$, each of which is built up from MoO_6 octahedra, PO_4 tetrahedra, and pyrophosphate groups P_2O_7, the silver compound is composed only of MoO_6 octahedra and P_2O_7 groups. In $AgMo_5P_8O_{33}$, $Mo(1)O_6$ and $Mo(2)O_6$ octahedra share their five corners with four P_2O_7 groups with the sixth corner being unshared. One of the four P_2O_7 groups shares two oxygen atoms with the MoO_6 octahedron. The coordination polyhedra around Mo1 and Mo2 are distorted and are similar to those observed in the cesium and the potassium compounds. The Mo3 atom is located on the two-fold axis and infinite chains parallel to the *b* axis are formed by distorted $Mo(3)O_6$ octahedra linked together by sharing the opposite corners. However, the coordination polyhedron of Mo3 is much more distorted than those of Mo1 and Mo2. It is coordinated by five oxygen atoms at distances around 1.95 Å with the sixth oxygen atom at 2.94 Å (Fig. 6). As observed in $MoOPO_4$ (*6*), the distortion is so pronounced that a description in terms of a square pyramidal arrangement of oxygen atoms around Mo3 is more appropriate, but unlike $MoOPO_4$, which has one short, one long, and four intermediate length Mo–O bonds, the Mo3 environment contains one long and five intermediate length bonds. The pyrophosphate groups, $P(1)P(2)O_7$ and $P(3)P(4)O_7$, are similar in both configuration and P–O–P bond angle to those in $Cs_4Mo_8P_{12}O_{52}$. Each pyrophos-

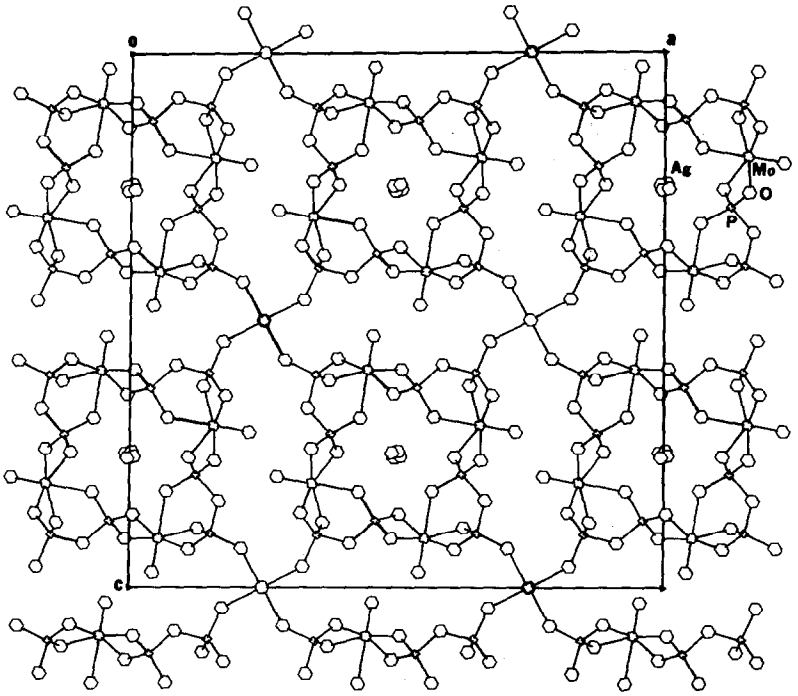

FIG. 4. $AgMo_5P_8O_{33}$ structure as viewed along the *b* axis.

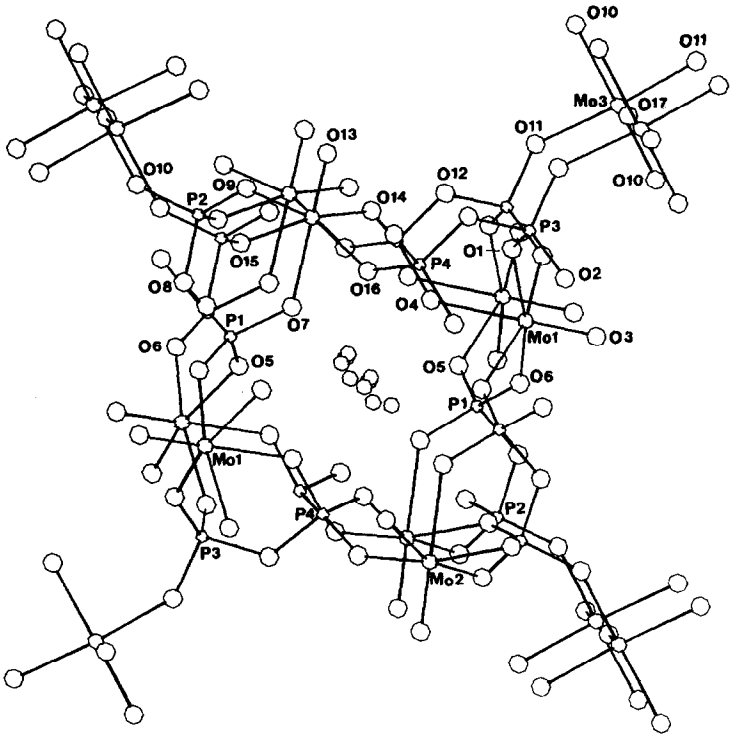

FIG. 5. A perspective view of the tunnel in $AgMo_5P_8O_{33}$.

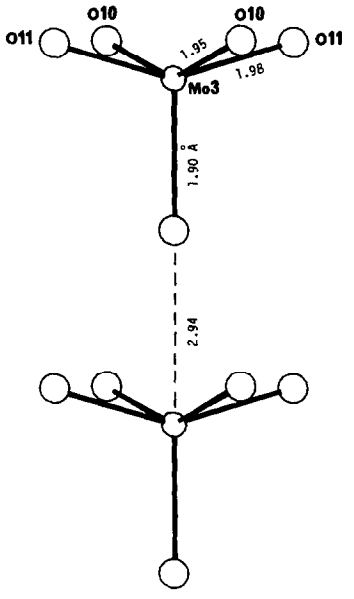

FIG. 6. The coordination of oxygen atoms around Mo3 in $AgMo_5P_8O_{33}$.

phate group shares its six corners with four MoO_6 octahedra and one $Mo(3)O_5$ square pyramid. One of the four MoO_6 octahedra shares two oxygen atoms with the pyrophosphate group. Based on the above discussion, the connectivity formula for $AgMo_5P_8O_{33}$ is $Ag(MoO_{1/1}O_{4/2})(MoO_{1/1}O_{5/2})_4(P_2O_{1/1}O_{6/2})_4$.

As mentioned above, there are two major Ag sites in the asymmetric unit, each of which is 25% occupied. Since there are four possible sites for Ag atoms in each tunnel, there is one Ag atom in each tunnel per unit cell (see Fig. 7). The neighboring Ag sites are too closely spaced (d(Ag1–Ag2) = 1.38, 1.09 Å) to be simultaneously occupied. Because there is no evidence of doubling along any one of the three axes, the silver atom could be disordered among the four possible sites. The temperature factors parallel to the tunnel direction for both of the

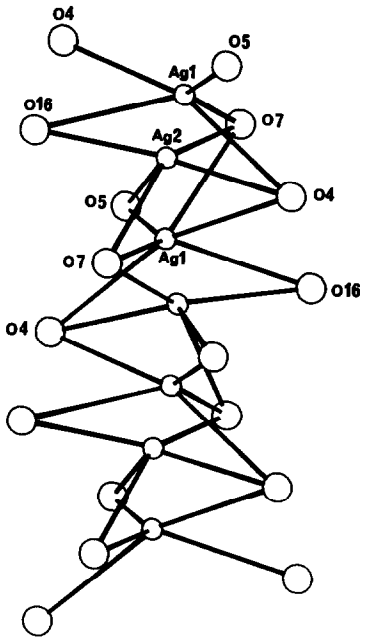

FIG. 7. The coordination of oxygen atoms around the silver sites in $AgMo_5P_8O_{33}$. Each silver site is only 25% occupied.

Ag atoms are large, suggesting additional positional disorder along the tunnel. Accordingly, this compound shows some structural characteristics that are required for ionic conductivity: (a) There are empty sites available for the Ag ions to diffuse into. (b) As shown in Fig. 7, both the Ag1 and Ag2 sites have similar coordination environments, indicative of a low activation energy barrier for jumping between neighboring sites. (c) The structure contains tunnels with a diameter of about 4.5 Å through which the Ag ions should easily migrate. However, a crystal of $AgMo_5P_8O_{33}$ with a size suitable for conductivity measurements has not been obtained.

The disorder on the Ag sublattice may be responsible for the featureless antiferromagnetic ordering which appears to be occurring below 2.5 K from Fig. 2. Normally, in a crystallographically well-ordered compound with a three-dimensional array of magnetic ions, magnetic ordering is of long range and the transition manifests itself by a cusp in $\chi(T)$. Lattice disorder, as in a spin glass, typically smears out the transition in static susceptibility measurements. Here, even though the magnetic sublattice is well-ordered crystallographically, the interactions between the magnetic ions may be somewhat disordered due to the disorder on the Ag sublattice; this type of disorder is expected to have similar consequences for $\chi(T)$ as in the case of lattice disorder among the magnetic ions.

Since the ionic radius for Li^+ is considerably smaller than that of Ag^+ or Na^+, the existence of $LiMo_5P_8O_{33}$ is somewhat unexpected. On the other hand, the tunnel is able to accommodate the large divalent cation Ba^{2+}, although one would expect much higher electrostatic repulsion compared to Ag^+. Further research on the compounds containing divalent alkaline earth elements is well worthwhile, because they present the possibility of mixed-valence molybdenum phosphates.

References

1. K.-H. LII AND R. C. HAUSHALTER, submitted for publication.
2. A. LECLAIRE, J. C. MONIER, AND B. RAVEAU, *J. Solid State Chem.* **48,** 147 (1983). For additional references on other mixed framework materials see: A. LECLAIRE, J. C. MONIER, AND B. RAVEAU, *J. Solid State Chem.* **59,** 301 (1985); R. MASSE, M. T. AVERBUCH-POUCHOT, AND A. DURIF, *J. Solid State Chem.* **58,** 157 (1985); B. RAVEAU, *Proc. Indian Acad. Sci.* **96,** 419 (1986).
3. D. T. CROMER AND J. T. WABER, "International Tables for X-Ray Crystallography," Vol. IV, Table 2.2A, Kynoch Press, Birmingham, England (1974).
4. J. A. IBERS AND W. C. HAMILTON, *Acta Crystallogr.* **17,** 781 (1964).
5. D. T. CROMER, "International Tables for X-Ray Crystallography," Vol. IV, Table 2.3.1, Kynoch Press, Birmingham, England (1974).
6. P. KIERKEGAARD AND M. WESTERLUND, *Acta Chem. Scand.* **18,** 2217 (1964).